KMS Technologies – KJT Enterprises Inc.

Publication

Veeken, P. & Rauch-Davies, M.

2006

AVO attribute analysis and seismic reservoir characterization

First Break, 24, 41-52

AVO attribute analysis and seismic reservoir characterization

Paul Veeken[1]* and Marianne Rauch-Davies[2]

Introduction

This article summarizes some basic concepts in AVO processing and the computation of prestack seismic attributes. Seismic modelling forms the basis for understanding the seismic signature. It helps in the prediction of reservoir characteristics away from well control points. Reliable estimation of petrophysical parameters is needed as input for such studies. These petrophysical estimates are an integral part of more advanced reservoir characterization and modelling.

First, the AVO principles are described and various prestack attributes are presented. Subsequently, the elastic approach is discussed and finally the benefits of seismic modelling with advantages of multi-disciplinary reservoir studies are demonstrated.

Amplitude-versus-offset (AVO) principles

The amplitude character of seismic reflections varies with offset, due to changes in the angle of incidence. The common-depth-point (CDP) gather (Fig. 1a) shows the variation for different traces. Figure 1b illustrates the changes in the seismic response when a water-wet brine-filled reservoir is replaced by oil or gas. The synthetics are calculated along a normal incidence and zero offset trajectory. The hydrocarbon saturation is set at 80% (Robinson et al., 2005). Both hydrocarbon cases show brightening of the reflection with respect to the brine-filled scenario. The sands have lower acoustic impedance (AI) than the encasing shales. Not only the top reservoir reflection shows this increased contrast tendency, but the seismic loop directly below it also manifests considerable changes. Figure 2 illustrates a positive gas-sand reflection decreasing with offset, while the negative water-wet reservoir above shows less reflectivity change. The polarity of the data is normal, i.e. an increase in acoustic impedance with depth (or hard kick) corresponds to a peak to the right on the seismic traces. The two highlighted reservoirs are of differing petrophysical character and the encasing geology (compaction/lithology) changes with depth. Although this kind of amplitude variation is evident on the prestack CMP gathers, it has been somewhat ignored in the past by interpreters because they work primarily with the stacked migration data set.

Nowadays, special studies are conducted on a routine basis to analyse the behaviour of the 'amplitude-versus-offset' (AVO-studies). This type of data contains detailed infor-

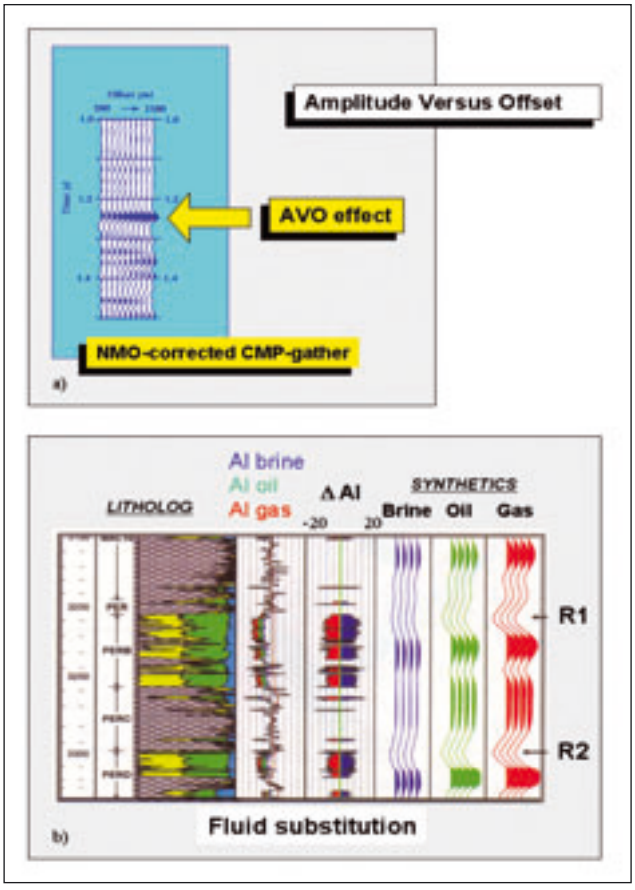

Figure 1 *(a) The AVO response on a reflection in a CDP gather. The amplitude changes clearly with offset (modified after Yilmaz, 2001, (b) Here, the fluid replacement effect on the seismic response is illustrated on a Pliocene lacustrine reservoir from the Chirag Field in the south Caspian Sea. The synthetics have been generated by applying Gassmann fluid substitution. Note how not only the top of the reservoir reflection changes but also the reflection just below. Analysis using window measurements can therefore help to discriminate between water- and HC-filled reservoirs. The top reservoir corresponds to a trough on the synthetic trace. The seismic traces are displayed with a positive polarity, whereby a decrease in AI corresponds to a negative trough. The reservoir sand has a smaller AI than the overlying shale (Robinson et al., 2005).*

[1] *Geops, 22 Rue Colonel Fabien M4, Antony 92160, France*
[2] *KJT enterprises - 6420 Richmond Avenue S-610, Houston, Texas 77057, USA*
* *pveeken@hotmail.com*

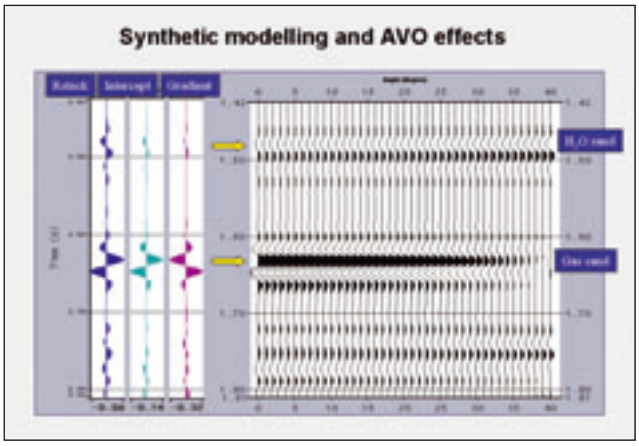

Figure 2 *AVO effect on a flattened synthetic CDP gather caused by the presence of gas in a reservoir sand. The near-offset amplitude value is different from the amplitude measured on the far-offset trace. Note the difference of the amplitude response in the water-filled reservoir above. The changes in the petrophysical characteristics of the encasing shale sequence with depth and the diagenesis are some of the causes for the different responses. If the gas were replaced by water in the same reservoir unit, the main change would occur in the zero-offset R_0 reflectivity, while the amplitude gradient is not necessarily affected as much.*

mation on the porefill of reservoirs (e.g. Ostrander 1984; Castagna and Backus 1993; Chiburis et al., 1993; Hilterman 2001; Veeken et al., 2002; Da Silva et al., 2004a). Ultimately it will lead to a more efficient evacuation of hydrocarbons with substantially improved recovery factors (Fig. 3).

The amplitude behaviour of the different raypaths also varies according to the porefill and lithology. Water-filled reservoirs often show variations in amplitude with offset that are different from those of hydrocarbon-filled reservoirs. The change in zero-offset reflectivity R_0, or intercept, is the most diagnostic feature. The seismic response depends on the encasing geology, porefill, and interference effects. It varies with depth and differs in various parts of the world. Studying the prestack differences in detail can indicate the causes of near- and far-offset amplitude variability (Fig. 4). The seismic signature from a gas sand is different from the brine-filled response when the same reservoir is observed under similar conditions. In such a situation, the encasing geology is probably the same and has little influence on the observed anomalous amplitude behaviour. A distinct change in zero-offset reflectivity is probably the most remarkable phenomenon. Changes in amplitude with offset can occur in hydrocarbon- as well as water-bearing reservoirs; in that case the intercept might contain the vital porefill information.

The AVO effect represents a potentially powerful tool to discriminate between water- and hydrocarbon-saturated reservoirs. However, it means going back to the prestack domain. It should be ensured that the data on individual CDP gathers come from a consistent subsurface location. This is generally achieved by a proper migration of the input data set (prestack time migration, Da Silva et al., 2004b). Careful data preconditioning is essential when quantitative interpretation is the ultimate aim (Veeken and Da Silva, 2004).

Reflection coefficients at different offsets

For a quick analysis, the reflection coefficients at different offsets and angles of incidence are usually computed. The correct procedure is to use the full set of Zoeppritz equations (Zoeppritz, 1919), but these are quite awkward to handle (Fig. 5). These equations yield amplitudes that are accurate up to the critical angle as their description does not include head-wave energy (Sheriff, 2002). The equations assume continuity of stress and displacement at the interface.

Aki and Richards (1980) gave a more convenient matrix description of the Zoeppritz equations and they produced the following formula:

$$R_{(\theta)} = 0.5\left(1-4p^2V_S^2\right)\left(\Delta\rho/\rho_a\right) + \left(1/2\cos^2\theta\right)\left(\Delta V_P/V_{Pa}\right) - 4\left(p^2V_{Sa}^2\right)\left(\Delta V_S/V_{Sa}\right) \quad (1)$$

where $\rho_a = (\rho_1+\rho_2)/2$, $\Delta Vp = (Vp_2 - Vp_1)$ and $p = \sin\theta_1/Vp_1 = \sin\theta_2/Vp_2$. The parameter p is also known as the ray parameter in Snell's law. The suffix a indicates average. V_P is the P-wave interval velocity and V_S is the S-wave velocity in m/s. The density is denoted by ρ and it is expressed in gm/cm^3. The suffix in brackets for the reflectivity R denotes the specific angle of incidence θ. $R_{(0)}$ is the zero-offset amplitude.

Shuey (1985) proposed a polynomial fit for the reflectivity that is accurate for an angle of incidence up to 35°, using Poisson's ratio σ:

$$R_{(\theta)} = R_{(0)} + \left[R_{(0)}V_0 + \Delta\sigma/\left(1-(\sigma_2-\sigma_1)^2\right)\right]\sin^2\theta + 0.5\left[\left(\Delta V_P/V_P\right)\left(\tan^2\theta - \sin^2\theta\right)\right] \quad (2)$$

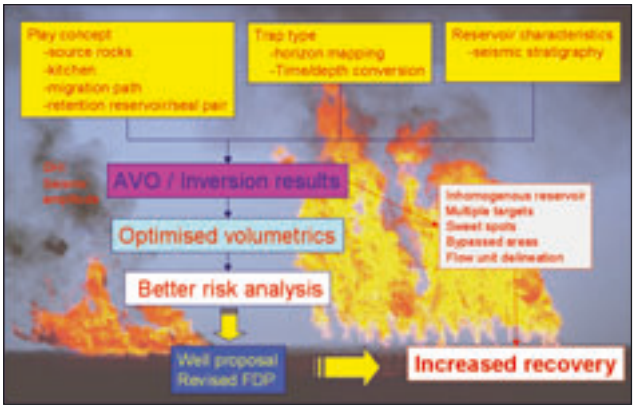

Figure 3 *Benefits of seismic attribute analysis on the hydrocarbon evacuation. The efficiency and the quantity of recovered reserves are increased, whilst the drilling risk is reduced. Sweet spots and multiple targets are identified at an early stage.*

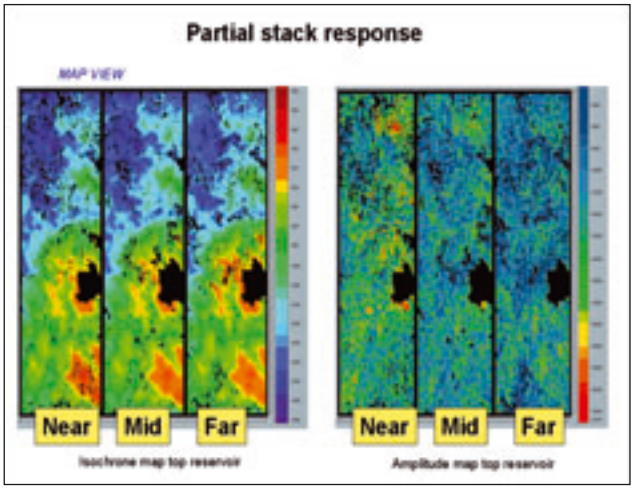

Figure 4 *Map view of partial stack response, showing isochrone and amplitude values of top reservoir. Differences between the partial stacks indicate the presence of AVO effects, but it is important to determine their origin. The small differences in the isochrone maps are related to residual moveout. The near-offset traces are in part stronger in amplitude than the far-offset traces and an investigation should be made into whether this is caused by possible porefill changes. The a-typical AVO behaviour is also related here to overlying shale package (data courtesy of TotalFinaElf).*

where

$$V_0 = A_0 - 2(1+A_0)\left[(1-2(\sigma_1+\sigma_2))/(1-(\sigma_1+\sigma_2))\right]$$
$$A_0 = (\Delta V_P / V_P)/(\Delta V_S / V_S + \Delta\rho/\rho)$$

Poisson's ratio is defined as the ratio of transverse contraction to longitudinal extension when a rod is stretched (Sheriff, 2002). The Shuey formula is often written in a simplified form:

$$R_{(\theta)} = A + B\sin^2\theta + C\sin^2\theta\tan^2\theta \qquad (3)$$

The formula can be rewritten assuming $(\sigma_1+\sigma_2)/2 = 0.33$ $(\rightarrow V_0 = 1)$ and $V_P/V_S = 2$. In this case, the higher terms can be dropped by limiting the angle of incidence to $\theta < 30°$. We then have

$$R_{(\theta)} = R_{(0)} + \left[2.25(\sigma_2-\sigma_1) - R_{(0)}\right]\sin^2\theta = R_{(0)} + G\sin^2\theta \qquad (4)$$

where $R(\theta)$ denotes the P-wave amplitude or reflectivity at angle of incidence θ; $R_{(0)}$ denotes the P-wave amplitude at θ = 0 (zero offset), also known as the intercept I; and G denotes the gradient (or slope) of the line that approximates the reflectivities at different offsets in a crossplot of R_P versus $\sin^2\theta$. A positive gradient means that the amplitude increases with offset.

According to Hilterman (2001), the Shuey formula can be represented in yet another simpler form:

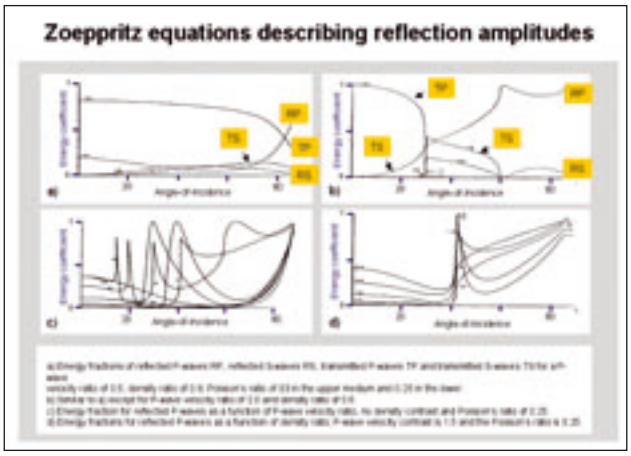

Figure 5 *Zoeppritz equations for computing the amplitude of the different raypaths in a layered medium. The head-wave energy is not considered in this approach and therefore the amplitudes are only correct up to the critical angle (modified after Sheriff, 2002).*

$$R_{(\theta)} = R_{(0)}\cos^2\theta + PR\sin^2\theta \qquad (5)$$

where PR denotes Poisson's reflectivity. Poisson's reflectivity is defined as

$$PR = (\sigma_2-\sigma_1)/\left(1-((\sigma_1+\sigma_2)/2)\right) \qquad (6)$$

where σ^1 and σ^2 are Poisson's ratio in media 1 and 2, respectively. This PR is approximately equal to $4R_{(30)} - 3R_{(0)}$. In a crossplot of 0.5 ln(AI) versus Poisson's ratio, it appears that the lithologies plot on a linear trend, with slope $R_{(0)}/PR$.

The reflectivity of each time sample in the various offset cubes is computed and examined. The common-midpoint (CMP) gather is scanned for variations in the amplitudes with offset. A linear regression analysis is carried out to compute the

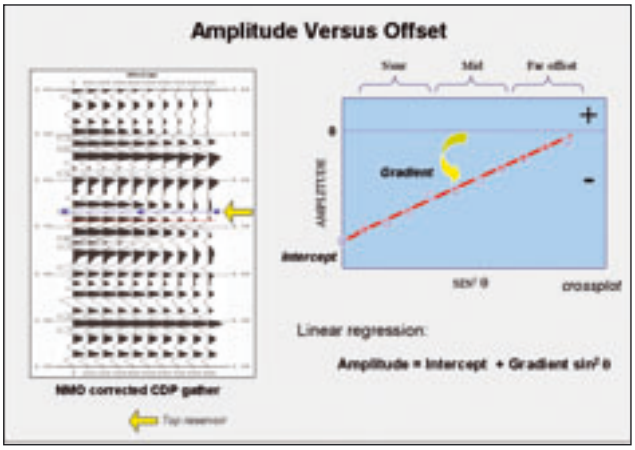

Figure 6 *AVO attributes computed in an amplitude-versus-$\sin^2\theta$ crossplot. The regression line gives the intercept I (cut-off on the Y-axis) and the gradient G (the slope of the line) that defines the rate of change in amplitude with offset.*

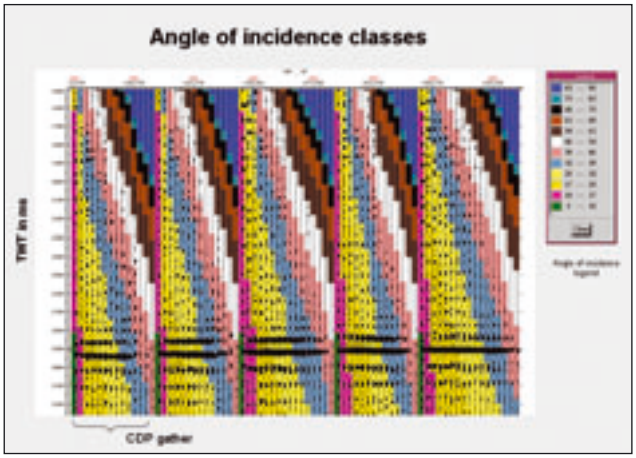

Figure 7 *CMP gathers with different colours indicating the various angle-of-incidence ranges. Simple 2D ray-tracing is often used for conversion from offset to angle of incidence.*

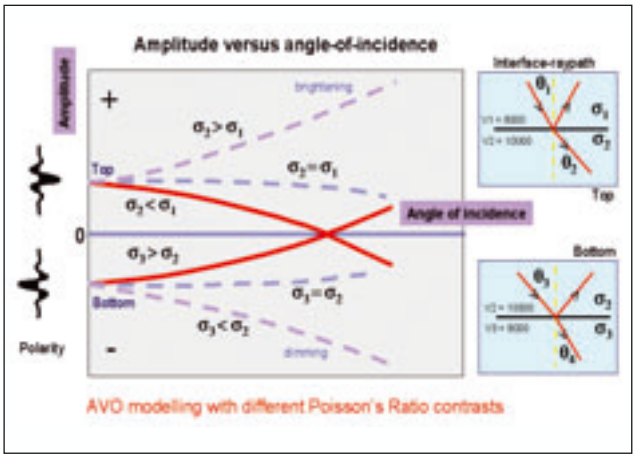

Figure 8 *AVO response at the top and base of a hypothetical lithological unit. Poisson's ratio σ is equal to the ratio of transverse contraction to the longitudinal extension and it governs the AVO effect.*

intercept I (cut-off on the amplitude axis: R_0) and the gradient G (slope of the regression line) in a crossplot of amplitude versus $\sin^2\theta$, where θ is the angle of incidence. The physical meaning of the AVO attributes I and G is shown in Fig. 6. This crossplotting technique means that the data is converted from the offset domain into the 'amplitude versus angle-of-incidence' domain (AVA). This is usually done by simple 2D ray-tracing, applying Snell's law at the interfaces and using interval velocities from the smoothed normal moveout (NMO) velocities (Fig. 7). A three-point attribute computation, with a near, mid and far determination, is usually adequate and cost-effective (Rauch-Davies and Portniaguine, 2004). The theoretical response at the top and bottom of a reservoir unit is shown in Fig. 8. The difference in Poisson's ratio over the interface will result in a different behaviour of the stack (brightening or dimming effect). Cambois (2000a) demonstrated that processing steps may adversely influence Poisson's ratio as deduced from P-wave seismics. Careful quality control is certainly advisable. Processing steps, such as amplitude recovery, gain control, NMO stretch, and residual NMO, introduce additional uncertainties into the determination of Poisson's ratio (Cambois 2000b). Their negative effects are difficult to counterbalance later on (Fig. 9).

AVO attributes analysis

For AVO analysis it is standard practice to calculate an I*G attribute (intercept*gradient), which is equal to a simple multiplication of the two fundamental AVO attributes. The results are often represented in 'product stack' sections, that allow convenient inspection of the behaviour. Also a fluid factor (FF) attribute is computed (Fig. 10). This FF attribute can be established in several ways:

(a) *I – G crossplot method*

The attribute is based on a weighted function that will place I and G in similar value ranges. These values are then crossplotted and in this new (I – G) plot, the difference from the so-called "wet-rock line" is determined (Fig. 11). The wet-rock line is equivalent to the lithology trend or mudrock line of other authors. The difference in distance of the individual points to the wet-rock line is the fluid factor. The wet-rock line represents the central regression line through the cloud of data points (Foster et al., 1993; Ross, 2000; Veeken et al., 2002). The gas-filled-reservoir points are plotted significantly further away from this regression line. The plot has a typical butterfly shape: a lot of points along the central-line trend with two clouds of points positioned symmetrically around it.

(b) The V_P–V_S crossplot method

In the V_P–V_S plot, the mudrock line is established and the residual error in a least-squares sense is a measure of the fluid factor (Smith and Gidlow 1987; Smith and Sutherland 1996), given by

$$FF = -1.16R_P(V_S/V_P)R_S \quad (7)$$

where R_P is the P-wave reflectivity and R_S is the S-wave reflectivity. It is possible to use a local or a fixed slope for the mudrock line, like that deduced by Castagna et al. (1985):

$$V_P = 1.16V_S + 1360 \text{ m/s}. \quad (8)$$

Rp varies with angle of incidence. Linear regression in the AVO (R_P–$\sin^2\theta$) crossplot gives R_P at $\theta = 0$, and this is known as the intercept I. When $V_P/V_S = 2$, then for an angle of incidence of 0°, the two-term approximation is valid and (Russell et al., 2003):

$$R_P = \text{intercept},$$
$$R_S = (\text{intercept} - \text{gradient})/2 \quad (9)$$

As already mentioned, the AVO attributes are calculated for each time sample on the seismic trace from the flattened CDP gather. Prestack seismic attribute cubes are thus generated. These cubes are scrutinized for anomalies that may represent hydrocarbon-filled reservoirs. The correct interpretation of the AVO attribute cubes is a delicate art in itself.

AVO reservoir classification

Rutherford and Williams (1989) classified reservoirs, based on the amplitude behaviour of the top reflection as a function of offset. Castagna and Swan (1997) complemented the scheme with an additional fourth class (Fig. 12):

- Class 1 Large positive R_0 amplitude that remains positive (dimming of reflection on stack).
- Class 2 Small positive R_0 that is transformed into negative reflectivities with offset (dimming/brightening of reflection on stack and polarity flip).
- Class 3 Negative R_0 amplitude that becomes more negative (brightening of reflection on stack).
- Class 4 Negative amplitude becomes less negative with offset.

The angle of incidence is historically limited to 45° because at larger offsets the approximation of the Zoeppritz equations breaks down (cf. Sheriff, 2002). The main discriminator in this classification scheme is the relationship of the top reservoir with the overlying lithology and the changes in the seismic response of the top reservoir reflection. A disadvantage of this system is that the classification depends on the offset range which changes from survey to survey. Longer offsets are the tendency today and hence a former Class 1 sand might suddenly become Class 2, as negative values are now seen on the far-offset traces of the new seismic data set.

Let's analyze the behaviour of a Class 3 gas sand in more detail. The top of a gas-filled Class 3 sand has a positive I*G (negative gradient and negative intercept) and its base is also positive (positive gradient and positive intercept). FF (computed from I and G) has a negative value at the top and a positive value at the base of the gas reservoir. The sections through the two AVO attribute cubes are now examined for the presence of these dual anomalies. For quick identification, it is useful to display I*G as a density colour, whilst FF is overlaid as a wiggle trace in one TWT section. This is done in a so-called Nacho plot (Fig. 13).

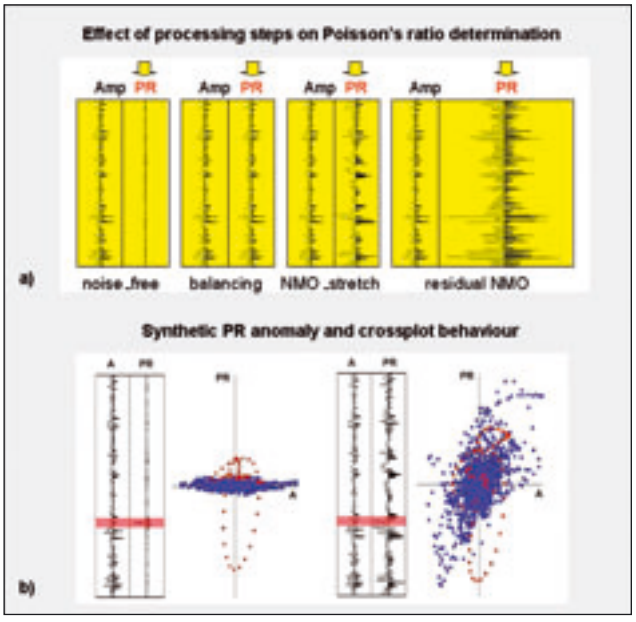

Figure 9 *(a) Data preconditioning is an important step when carrying out reservoir characterization studies. Standard processing steps can introduce significantly large changes in Poisson's ratio, as illustrated by Cambois (2000b). It will be very difficult to determine the exact change in Poisson's ratio from this type of seismic data. (b) Introduction of a synthetic PR anomaly in the noise-free data set. The anomaly stands out in the crossplot. After NMO stretch and with noise, the red dots are blended with the background in the corresponding crossplot, making it very difficult to retrieve the original anomaly in the Poisson's ratio.*

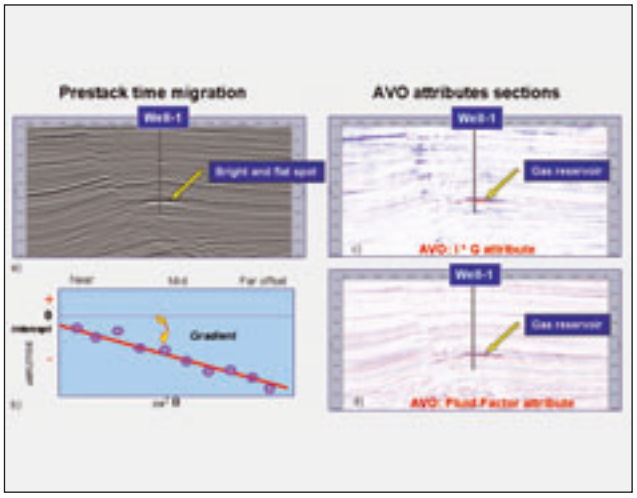

Figure 10 *(a) Amplitude section with distinct flat spot, caused by the presence of gas in a reservoir. It also corresponds to clear anomalies in the I* G and the FF AVO attributes, as shown in the two figures below (data courtesy of Pemex). (b) (amplitude-versus-sin^2) crossplot and regression line defining intercept and gradient: amplitude = intercept + gradient * sin^2. (c) I*G attribute computed from the amplitude-versus-sin^2 crossplot. The intercept I, or R_0, is the cut-off value for the amplitude at zero angle of incidence. The gradient is the slope of the regression line through the amplitude points at the different angles of incidence. (d) The fluid factor (FF) attribute is a weighted function between the intercept and gradient attributes. The 'wet-rock' line is established in a crossplot (see Fig. 11) and the distance from the individual points to this line gives a measure of the fluid factor.*

The following logarithmic attribute (gas indicator GI) is suggested for detecting gas in Class 2 sands:

$$GI = \text{intercept}^* (1n(\text{abs}G)) \quad (10)$$

This attribute is specially designed for the Gulf of Mexico region; world-wide application requires local adjustment (Fig. 14).

Sign of AVO effects and dual attribute anomalies

		I	*G*	*I*G*	*FF*	*GI*
Class 3 reservoir	top	–	–	+	–	
	base	+	+	+	+	
Class 2 reservoir	top	+	–	–		+
	base	+	+	+		+

For the discrimination of Class 2 gas sands, Verm and Hilterman (1995) proposed taking the Shuey equation and assuming that $V_P/V_S = 2$ (higher-order terms can be neglected) and $\sigma = 0.33$. This gives:

$$R_{(\theta)} = R_{(0)} + \left((9/4)^* \Delta\sigma\right) - R_{(0)} \sin^2\theta \quad (11)$$

They then used a crossplot of Poisson's reflectivity (or *PR*) versus the normal incidence reflectivity (R_0) to discriminate anomalies caused by the Class 2 sands.

Class 1 and Class 4 sands are not so commonly reported on. The AVO effect depends on the combination of the petrophysical properties of the overlying lithology and the reservoir rock (V_P, V_S and ρ). The impedance contrast over the top reservoir interface is the critical factor. Normal polarity means that an increase in acoustic impedance (or a hard kick) is represented by a positive peak on the seismic data. Class 1 is a response with a relatively high positive intercept and a decrease in the amplitude with offset (negative G). It is often related to tightly compacted reservoirs and/or reservoirs with a high velocity/density cement (cf. Odegaard and Avseth, 2004; Roden et al., 2005). However, it is the impedance contrast that is important, and it may equally well reflect the fact that the overlying lithology is very slow and not very dense. Although many authors have suggested a deep-seated compacted reservoir for this type of AVO response and consequently a relatively old geological age for the rocks concerned, Class 1 reservoirs may occur at any depth.

A Class 1 AVO response has been described for Tertiary sediments in the offshore part of the Nile delta in Egypt (Marten et al., 2004). Brightening of gas-filled Class 1 reservoirs in the Pliocene H'apy Field, offshore Egypt, has been reported by Wigger et al., (1997). Seal integrity is an aspect that is often ignored when analyzing the seismic expression of a gas reservoir. A perfect seal hardly ever exists and therefore some chimney effect due to hydrocarbon leakage will occur. This will change the petrophysical properties of the top seal directly above the reservoir. This phenomenon may lead to an unexpected AVO behaviour and brightening of a Class 1 reservoir when gas filled. It is important to check the polarity of the data set before drawing any conclusions about the AVO reservoir classification. A reliable well–to-seismic tie is, in this respect, certainly strongly recommended.

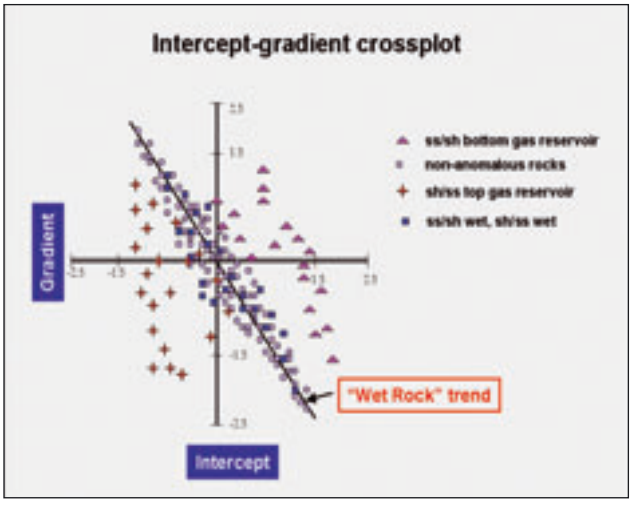

Figure 11 *Crossplot between intercept and gradient. The axis has been weighted by a simple multiplication factor to bring the two attributes closer in line with each other. The regression line is the 'wet-rock' line and the distance to this line determines the fluid factor value. The shape of the point cloud typically resembles a butterfly outline (positive and negative values outside main trend) when hydrocarbons are present.*

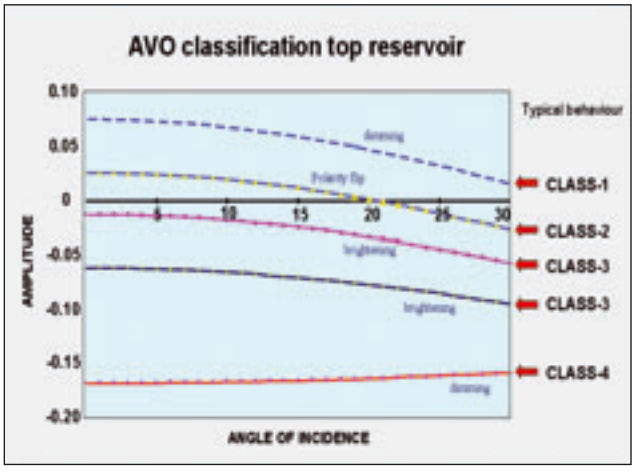

Figure 12 *Classification of reservoirs based on the AVO response of the top boundary interface. The stacked trace will show brightening, polarity flip or dimming with respect to the zero-offset trace. The classification depends on the contrast of petrophysical properties of the reservoir rock with the overlying unit. In the case of a non-perfect top seal, the properties of the overlying unit can also change when the reservoir is gas filled.*

Class 4 is characterized by high negative impedance that shows little difference with offset. It may coincide with the behaviour of shallow burial, unconsolidated sands. Here, the decrease in negative amplitude with offset, when gas is present in the reservoir, can be partly caused by the above-mentioned seal-integrity problem. The overlying high-velocity lithology (shale/siltstone or carbonate) may have a V_S that is higher than that of the reservoir (Roden et al., 2005). The P-wave velocity drop at the interface is often of the order of 700 m/s (Rauch and Craig, 1998).

It is noteworthy that unconsolidated sands are even encountered at great depths: below 4700 m. For example in the Ek Balam discovery well (GOM, offshore Campeche), Upper Oxfordian sabkha sands are penetrated that are unconsolidated in the recovered core (G.A. Velasco Vasquez, pers. comm.; Pemex 2000). These sabkha sands were probably prone to very early cementation with gypsum. In the ongoing burial and compaction, this cement was not stable and it dissolved at greater depths, thus creating an anomalous porosity/permeability distribution. The unconsolidated nature of these sands at such an extreme depth was an unexpected discovery for the drillers and the geologists.

The fact that the propagation velocity of a waveform is direction-dependent is called anisotropy. The simplest case of anisotropy is polar anisotropy or transverse isotropy (one axis is different whilst the property is the same on the other two axes). Polar anisotropy is thus uni-axial anisotropy and the axis can be vertical, tilted or horizontal (Jones et al., 2003). Vertical transverse isotropy (VTI) is mainly the result of variations in the geological layering. Horizontal transverse isotropy (HTI) is used for quantifying the amount and direction of vertical fracturing, for instance (cf. Hilterman, 2001). It causes azimuthal anisotropy in the seismic data (Lynn, 2004). The azimuth of the anisotropic gradient indicates the fracture orientation. It depends on fracture aperture, fracture density and directional permeability. Todorovic-Marinic et al., (2004) proposed a new attribute called 'the envelope of the anisotropic gradient' to visualize this HTI behaviour.

Of course, anisotropy effects also influence the AVO response (e.g., Jenner, 2002; Williams and Jenner, 2002). Jenner introduced a linear fit to correct the traveltimes for azimuthally varying NMO effects (NMOA). Analysis of amplitude with varying offset and azimuth resulted in another linear fit that enabled a correction to be calculated and this resulted in more accurate AVOA analysis.

As can be seen from the above discussion, it is important to establish which types of AVO reservoirs are expected in the area under investigation. This makes it possible to concentrate quickly on particular scenarios and perform case-specific analysis. There is, however, a severe danger of ignoring the fact that several types of AVO reservoirs might co-exist at the same time. Evaluating all options makes the evaluation of the AVO response more time consuming, but it will ensure that all plausible reservoir configurations are considered.

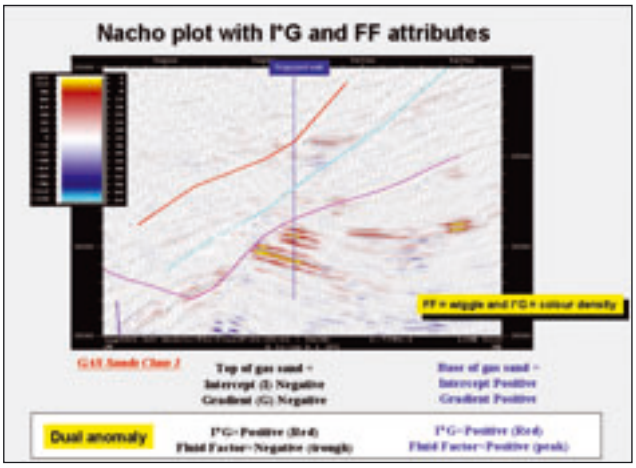

Figure 13 *A Nacho plot in which the I*G AVO attribute is displayed as a coloured density overlain by the FF attribute as a wiggle trace. It allows quick identification of interesting dual anomalies for Class 3 reservoirs (data courtesy of Pemex).*

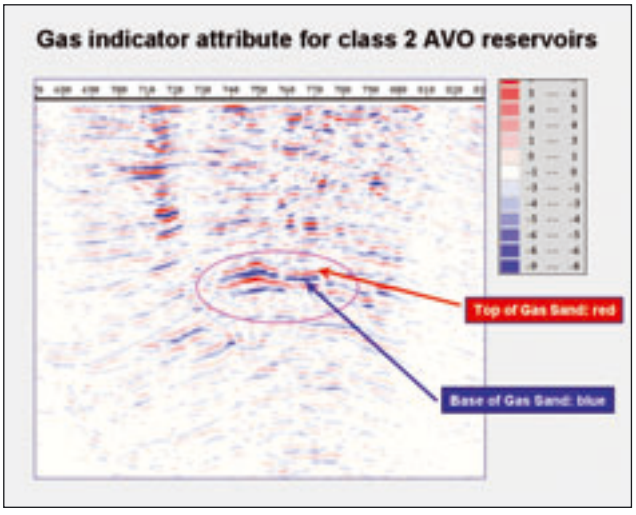

Figure 14 *Gas indicator (GI) for Class 2 AVO reservoirs in the Gulf of Mexico, where GI = I * (ln (abs(G))). The gas indicator attribute is derived for this particular seismic survey only, and its application to other areas requires verification of its validity. Tailor-made local adjustments are probably required to get a good separation for the HC reservoirs (data courtesy of Pemex).*

Elastic approach to the angle-dependent reflectivity

The elastic approach takes into account the behaviour of both P- and S-waves. It provides better discrimination of the effects caused by the changes in porefill, and the AVO behaviour is more accurately modelled (Veeken and Da Silva, 2004). The V_P/V_S attribute gives better separation at the top of the HC interval compared to V_P alone (Fig. 15).

The Shuey equation (Shuey, 1985) describes an approximation of the Zoeppritz reflectivity that is valid for angles

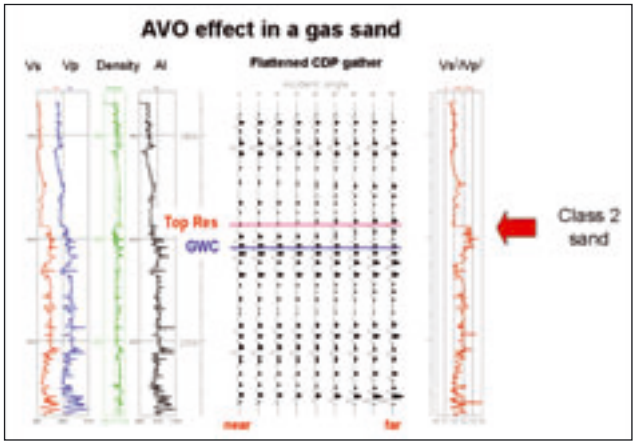

Figure 15 *AVO effect caused by the presence of hydrocarbons in a Class 2 type reservoir. The $(V_S/V_P)^2$curve best describes the HC interval. It demonstrates the benefits of adopting an elastic approach towards reservoir characterization.*

of incidence up to 30–35°. The assumption is made that V_P is approximately twice V_S and the higher terms are dropped under the 30° angle-of-incidence condition. When working with prestack data, it is necessary to obtain a better estimate and to take into account the difference between V_P and V_S. This is done in the so-called elastic approach. Connolly (1999) introduced the concept of elastic impedance, a seismic attribute that is angle dependent. He defined a function F(t) that is angle-of-incidence dependent and related to the P-wave reflectivity as follows:

$$R_{(\theta)} = \left(F(t_i) - F(t_{i-1})\right) / \left(F(t_i) + F(t_{i-1})\right) \quad (12)$$

The function F(t) is now called the elastic impedance, in analogy with the acoustic impedance concept. The angle-dependant P-wave reflectivity is also approximated by the simplified description of the Zoeppritz equations (Aki and Richards, 1980):

$$R_{(\theta)} = A + B\sin^2\theta + C\sin^2\theta\tan^2\theta \quad (13)$$

where

$$A = 0.5\left(\Delta V_P / V_P + \Delta\rho / \rho\right)$$

$$B = 0.5\left(\Delta V_P / V_P\right) - 4\left(V_S / V_P\right)^2\left(\Delta V_S / V_S\right) - 2\left(V_S / V_P\right)^2\left(\Delta\rho / \rho\right)$$

$$C = 0.5\left(\Delta V_P / V_P\right)$$

$$\Delta V_P = V_{P2} - V_{P1}$$

$$V_P = V_{P1} + V_{P2} / 2$$

A is the Intercept, B is the Gradient in AVO analysis and C is known as the AVO curvature.

Combining (12) and (13), we obtain the elastic impedance (*EI*) as:

$$EI_{(\theta)} = V_P^{(1+\tan^2\theta)} \cdot V_S^{(-8K\sin^2\theta)} \cdot \rho^{(1-4K\sin^2\theta)} \quad (14)$$

where K is a constant equal to the average of $(V_S/V_P)^2$. This type of *EI* computation is performed on the prestack gathers and takes into account the changes in V_P, V_S and density as well as AVO effects. The approach is accurate for small to moderate impedance changes. If the third term in the Shuey equation is dropped, then the $\tan^2\theta$ is simply replaced by $\sin^2\theta$ in the Connolly equation:

$$EI_{(\theta)} = V_P^{(1+\sin^2\theta)} \cdot V_S^{(-8K\sin^2\theta)} \cdot \rho^{(1-4K\sin^2\theta)} \quad (15)$$

The following assumptions have to be made:

- that the two-term NMO approximation is correct
- that Dix's equation is valid. His formula is generally accepted as a transform of stacking into interval velocities (Dix, 1955)
- that amplitudes are approximately proportional to $\sin^2\theta$. These conditions translate in a layer-cake geometry, an offset smaller than the depth of the reflector, an angle of incidence θ less than 30–35°, a transverse isotropic medium and, of course, correctly balanced prestack amplitudes. The ideal input consists of amplitudes that are directly proportional to the subsurface reflection coefficients without any additional distortions (Veeken and Da Silva, 2004). This is the main aim of 'preserved amplitude' processing. EI_0 corresponds to the acoustic impedance *AI* (= $\rho^* V_P$) and if *K* = 0.25, then $EI_{90} = (V_P / V_S)^2$.

The *EI* seismic attribute is the basis for performing an elastic inversion that is similar to acoustic impedance inversion

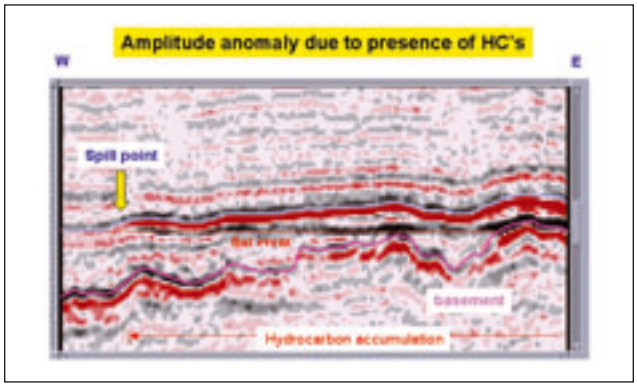

Figure 16 *A flat event resulting from the presence of hydrocarbons in a reservoir sequence. Wells have proved the HC accumulation. Synthetic modelling is helpful for understanding the seismic signature and it facilitates the interpretation of the seismic data. Fluid substitution, water saturation, porosity, net-to-gross, reservoir thickness and encasing lithologies are all parameters that can be changed to visualize their possible impact (data courtesy of TotalFinaElf).*

processing. One popular approach to acoustic impedance inversion estimates a wavelet (shaping filter or cross-correlation techniques) from the AI trace at the well and the seismic trace at the same location. In the elastic inversion, wavelets are derived for different angle-of-incidence traces of $EI(\theta)$ and the corresponding partial stack trace. There are other formulae that approximate the elastic impedance, e.g. the logarithmic approach or also a less common non-linear function (Tarantola, 1984, 1986; Pica et al., 1990). The logarithmic function avoids tedious exponential descriptions and is valid under the condition that K = 0.25, i.e.

$$\ln\left(EI_{(\theta)}\right) = \ln\left(I_P\right) + \left(2\ln\left(V_P/V_S\right) - \ln\left(I_P\right)\right)\sin^2\theta \qquad (16)$$

where

$$I_P = \rho * V_P$$

These formulae all have their own assumptions and validity range. This means that the elastic inversion results are suited for qualitative evaluation, but the absolute value of the inversion is not necessarily correct.

Extended elastic impedence (*EEI*) is a concept introduced by Whitcombe et al., (2000) and it is shown to correlate better with the various elastic parameters such as bulk modulus, shear modulus and λ, depending on the angle φ. The *EEI* is obtained by substituting $\tan\varphi$ for $\sin^2\theta$ in the Aki and Richards (1980) approximation of the Zoeppritz equations, where φ ranges between –90° and +90°. A normalization procedure is implemented in the extended elastic impedance approach (Rauch-Davies and Portniaguine, 2004). The *EEI* attribute is given by

$$EEI_{(\varphi)} = V_{PA}\rho_A\left[\left(V_P/V_{PA}\right)^a\left(V_S/V_{SA}\right)^b\left(\rho/\rho_A\right)^c\right] \qquad (17)$$

where
a= $\cos\varphi$.+ $\tan\varphi$,
b= –8K$\sin\varphi$,
c= $\cos\varphi$ – 4K $\sin\varphi$.
V_{PA}, ρ_A, V_{SA} are average values for V_P, ρ and V_S over the interval of interest. K is equal to the average value of $(V_S/V_P)^2$.

The angle φ = 0 corresponds to the AI value (Whitcombe et al,. 2000). The correlation of EEI with the gamma-ray log is useful for lithological discrimination (Neves et al., 2004). They suggested computation of a weighted stack to make a comparison between *EEI* and the seismic data possible. A frequency difference between near and far angle stacks is observed, with the far trace response being of lower frequency; hence they justify the filtering of the cubes to a similar amplitude spectrum.

Reservoir characterization

Reservoir characterization studies cover specific aspects of the reservoir development. In many cases it brings together data collected by different study techniques to describe the rocks under investigation in more detail. Seismics is the main data source away from the borehole calibration points; hence it is extensively used in lateral prediction studies and volumetric estimations. Integration of prestack data adds more information and that is why AVO or seismic inversion is so important for complementing the conventional approach. Some topics related to the prediction of petrophysical parameters from seismics and seismic attributes are presented below.

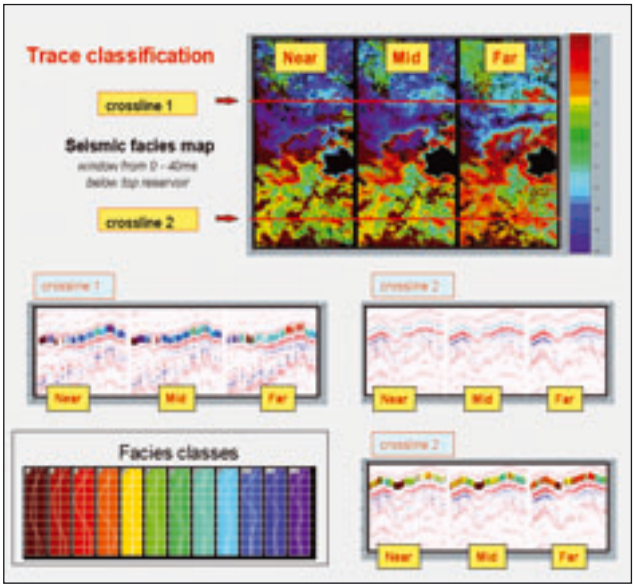

Figure 17 *A neural-network trace classification has been applied on the near-, mid- and far-offset partial stacks. The representative traces for the classes (master trace) are shown in the left-hand corner below. This shows that the signature changes significantly over the study area. The colour-coded classification for each trace is plotted along the top reservoir horizon in the cross-sections displayed. A supervised classification scheme will greatly facilitate the interpretation of the results (data courtesy of TotalFinaElf).*

Relationship of the linearized Zoeppritz approximation with some rock physical parameters

Dong (1996) and Whitcombe et al. (2000) showed, when using the linearized Zoeppritz equation (see equation (2)), that

$$\Delta\text{bulk modulus} = \left(3A + B + 2C\right)V_P^2\rho/1.5 \qquad (18)$$

It is difficult to deduce C from the seismic data set. Shuey (1985) therefore examined the behaviour of the ratio C/A in closer detail, and noticed that it ranges roughly between 0 and 1. The ratio C/A depends on the rock properties of the area under investigation. If it is 0.8 then it follows Gardner's relationship (Gardner et al., 1974). If it is assumed that the average values for the bulk modulus and $V_P^2\rho$ are constant, the above formula can be rewritten as

$$\Delta\text{bulk modulus} = A + B/\left(3 + 2\left(C/A\right)\right) \quad (19)$$

This function can be seen as analogous to the basic AVO equation:

$$R_\theta = A + \sin^2\theta \quad (20)$$

where

$$\sin^2\theta = 1/\left(3 + 2\left(C/A\right)\right)$$

This analogy translates the behaviour of the ratio C/A in terms of angle of incidence, so that:

C/A = 0.8 ==> $\sin^2\theta$ = 0.22 ==> θ =28°

Values of 0.5 and 1.6 have been encountered for C/A and these correspond to angles of 44° and 23° (Whitcombe *et al.* 2000). A similar treatment for λ can be carried out and this yields:

$$\Delta\lambda = 1/\left(2 + C/A\right) \quad (21)$$

Using Gardner's relationship, the results are $\sin^2\theta$ = 0.36 and the angle is 37°. The shear modulus relationship, according to Dong (1996), is as follows:

$$\Delta\mu = \left(C - B\right)\left(V_P^2\rho/2\right) \quad (22)$$

When C/A = 0, then Δμ is proportional to B. The equation can be rewritten as:

$$\Delta\mu = A - B/\left(C/A\right) \quad (23)$$

Using Gardner's relationship again and C/A = 0.8, it results in $\sin^2\theta$ = 1.25. This is physically meaningless and no angle of incidence θ can be computed. However Δμ can still be derived from a weighted difference of partial stacks or intercept–gradient stacks.

These relationships are valid under certain assumptions; when these are not adhered to, then the relationship breaks down. Linearization can only be carried out for small angles of incidence (<35°) and when impedance contrasts are relatively small.

Reservoir modelling and fluid substitution

Forward modelling should be seriously considered when possible direct hydrocarbon indicators (DHIs) are seen on the seismic data (Fig. 16). The modelling provides a better understanding of the data set. For this purpose, certain assumptions are made about reservoir parameters, such as: porosity, permeability, pore contents and geometry.

The initial reservoir-hostrock model is generally based on the well-log response (e.g. V_P, V_S and R_{hob}). The model is convolved with a seismic wavelet and a synthetic seismic section is generated. This synthetic section is compared with the original seismic line and similarities and/or discrepancies are detected. If well control is available, then it is possible to estimate the wavelet more correctly and generate more accurate synthetic traces. Fluid substitution is carried out to get an indication of the sensitivity of the seismic response to the presence of gas or water in the reservoir rocks. A simplistic Gassmann approach is often adopted, but be careful as this might give erroneous results when incorrect cut-off values for the logs are used (Skelt, 2004).

For computing petro-acoustic fluid substitution models it is necessary to make reliable estimates of V_P, V_S and the density ρ. The ratio V_P/V_S contains information about the lithology of the rocks (cf. Tatham, 1982). It also provides vital details on the fluid contents and is related to the porosity of the rocks. V_P and V_S both decrease with increasing porosity, with V_P decreasing twice as fast as V_S (Assefa et al., 2003). Under favourable circumstances, V_P and V_S can also provide information about the permeability of the rocks. Tsuneyama et al. (2003) demonstrated their relationship with the permeability and also the rock frame of carbonate rocks.

Constraints on modelling results

The modelling exercises provide valuable information on how to obtain a better fit with the measured data (iterative method with perturbation of the reservoir/seal properties). Data with different sample support should be integrated properly, with appropriate up- and down-scaling (cf. Nordahl et al., 2005). Indeed, seismic inversion provides a perception of some of the rock parameters, but the separate contributions of velocity and density are still difficult to substantiate. This knowledge will ultimately result in a better lateral prediction of the reservoir behaviour. It should be kept in mind that most of the time more than one solution exists for a given inversion problem. Other criteria have to be examined with regard to their usefulness in putting constraints on the number of solutions. Crossplot clustering, multi-attribute analysis, principal-component analysis and neural-network classification are promising techniques in this respect (Veeken, 2006). The automatic recognition of facies units, based on trace shape in a specific window around a mapped reservoir horizon, rapidly visualizes the subtle variations in seismic response (Fig. 17). The unsupervised approach is fast, but the result is somewhat ambiguous to interpret. The supervised approach is preferable as it generates a probability density function in each class, facilitating a direct interpretation. Multi-attribute 3D visualization and voxset rendering are excellent ways of presenting the results. However, there is a limitation to the method; i.e. the expected reservoir configuration can be modelled in various ways, but there always some basic assumptions are needed as primary input. The definitive answer can therefore only be found by drilling. Consequently, it is always advisable to quantify uncertainties connected with the modelled scenarios,

and to consider all plausible reservoir configurations (e.g. Brandstaeter et al., 2005; Klefstad et al., 2005; Rivenaes et al., 2005). Truly integrated studies with a shared earth model, material balance, production-history matching, flow simulation and real-time reservoir monitoring are needed from a reservoir management point of view. These types of interdisciplinary studies are the next step in modern asset management because they will reduce the drilling risks even further.

Conclusions

AVO effects on prestack CDP gathers provide basic information on the lithology and porefill contents of the rocks under investigation. The four-fold AVO classification is based on the seismic response of the top reservoir and depends on the acoustic impedance contrast over the interface, combined with interference effects.

Several AVO attributes are computed in an amplitude-versus-sin2θ crossplot using linear regression. The intercept I is the cut-off on the amplitude axis and the gradient G is the slope of the regression line. The attributes, I*G and fluid factor FF, are very helpful in quickly distinguishing Class 3 dual AVO anomalies, which are usually related to hydrocarbon-filled rocks. Customized combined I and G attributes may provide adequate differentiation to indicate the presence of hydrocarbons in Class 2 type reservoirs. Proper data preconditioning is an essential step, when quantitative interpretation is the ultimate goal.

Simplified reflectivity computations, valid under certain conditions, enable estimation of reservoir petrophysical parameters. The behaviour of both P- and S-waves is considered in the elastic approach. Prestack inversion incorporates modelling of the AVO effects and provides information about rock physical parameters such as Poisson's ratio, $\lambda\rho$, $\mu\rho$, V_P/V_S, I_P, I_S.

Reservoir modelling and fluid substitution increases understanding of the observed seismic response. It ultimately leads to a better lateral prediction with delineation of sweet spots and improved volumetric prognosis. This results in better reservoir management decisions, with augmented recovery factors and an improved drilling success ratio. Truly integrated studies will reduce the drilling and development risks even further.

Acknowledgements

This article is based largely on a textbook publication that is in press with Elsevier Scientific Publications: *Seismic Stratigraphy, Basin Analysis and Reservoir Characterisation* by P.C.H. Veeken. It will be part of the Handbook of Geophysical Exploration series, edited by K. Helbig and S. Treitel. Their kind permission to release the data for this publication is hereby acknowledged. Elsevier Scientific Publications is acknowledged for the copyright of this article.

The authors are grateful to CMG, Pemex and TotalFinaElf for use of their data. We thank our colleagues and the following persons for their contributions: J.L. Piazza, J. Guilbot, O. Bernet-Rollande, F. Pivot, O. Balz, G. Velasco Vazques, H. Bernal Ramirez, A. Marxh, I. Peres Negron, J. Camara, E. Mendez, D. Contreras Tebar, Q. Cardenas, R. Vila Villasenor, E. Guzman, R. Zaaki, M. Da Silva, G. Castillo, S. Addy, N. Van Couvering, W. Segovia, R. Martinez, and D. Gehant. Constructive comments by the reviewers were appreciated.

References

Aki, K. and Richards, P.G. [1980] *Quantitative Seismology, Theory and Methods*. W.H. Freeman & Co.

Assefa, S., McCann, C., and Sothcott, J. [2003] Velocities of compressional and shear waves in limestones. *Geophysical Prospecting* **51**, 1–13.

Brandstaeter, I., McIlroy, D., Lia, O., Ringrose, P., and Naess A. [2005] Reservoir modelling and simulation of Lajas Formation outcrops (Argentina) to constrain tidal reservoirs of the Halten Terrace (Norway). *Petroleum Geoscience* **11**, 37–46.

Cambois, G. [2000a] AVO inversion and elastic impedance. *70th SEG Meeting, Calgary, Canada,* Expanded Abstracts, 142–145.

Cambois, G. [2000b] Can P-wave AVO be quantitative. *The Leading Edge* **19**, 1246–1251.

Castagna, J.P. and Backus, M.M. [1993] *Offset Dependent Reflectivity – Theory and Practice of AVO Analysis*. Investigations in Geophysics No.8. SEG, Tulsa.

Castagna, J.P., Batzle, M.L., and Eastwood, R.L. [1985] Relationships between compressional and shear-wave in clastic silicate rocks. *Geophysics* **50**, 571–581.

Castagna, J.P. and Swan, J. [1997] Principles of AVO crossplotting. *The Leading Edge* **12**, 337–342.

Chiburis, E., Leaney, S., Skidmore, C., Franck, C., and McHugo, S. [1993] Hydrocarbon detection with AVO. *Oil Field Review* **5**, 42–50.

Connolly, P. [1999] Elastic impedance. *The Leading Edge* **18**, 438–452.

Da Silva, M., Rauch, M., Soto Cuervo, A., and Veeken, P.C.H. [2004a] Pre- and post-stack seismic attributes for enhancing production from the Cocuite gas reservoirs. *66th EAGE Conference, Paris, France,* Extended Abstracts, D001.

Da Silva, M., Rauch, M., Soto Cuervo, A., and Veeken, P.C.H. [2004b] Data conditioning for a combined inversion and AVO reservoir characterisation study. *66th EAGE Conference, Paris, France,* Extended Abstracts, P306.

Dix, C.H. [1955] Seismic velocities from surface measurements. *Geophysics* **20**, 68–86.

Dong, W. [1996] A sensitive combination of AVO slope and intercept for hydrocarbon indication. *58th EAGE Conference, Amsterdam, The Netherlands*, Extended Abstracts, M044.

Foster, D., Smith, S.W., Dey-Sarkar, S.K., and Swan, H.W. [1993] A closer look at hydrocarbon indicators. *63rd SEG Meeting, Washington, D.C., USA,* Expanded Abstracts, 731–733.

Gardner, G.H.F., Gardner, L.W., and Gregory, A.R. [1974] Formation velocity and density - The diagnostic basics for stratigraphic traps. *Geophysics* **39**, 770–780.

Hilterman, F.J. [2001] *Seismic Amplitude Interpretation*. SEG/EAGE short course no.4, Houston.
Jenner, E. [2002] Azimuthal AVO: methodology and data examples. *The Leading Edge* **21**, 782–786.
Jones, I.F., Bridson, M.L., and Bernitsas, N. [2003] Anisotropic ambiguities in TI media. *First Break* **21**, 31–37.
Klefstad, L., Kvarsvik, S., Ringas, J.E., Stene, J.J., and Sundsby, O. [2005] Characterisation of deeply buried heterolitic tidal reservoirs in the Smorbukk Field using inverted post-stack seismic acoustic impedance. *Petroleum Geoscience* **11**, 47–56.
Lynn, H.B. [2004] The winds of change; Anisotropic rocks – their preferred direction of fluid flow and their associated seismic signatures – Part I. *The Leading Edge* **23**, 1156–1162.
Marten, R., Shann, M., Mika, J., Rothe, S., and Quist, Y. [2004] Seismic challenges of developing the pre-Pliocene Akhen field, offshore Nile Delta. *The Leading Edge* **23**, 314–320.
Neves, F.N., Mustafa, H.M., and Rutty, P.M. [2004] Pseudo-gamma ray volume from extended elastic impedance inversion for gas exploration. *The Leading Edge* **23**, 536–540.
Nordahl, K., Ringrose, P., and Wen, R. [2005] Petrophysical characterisation of a heterolitic tidal reservoir interval using a process-based modelling tool. *Petroleum Geoscience* **11**, 17–28.
Odegaard, E. and Avseth, P. [2004] Well log and seismic data analysis using rock physics templates. *First Break* **22**(10), 37– 43.
Ostrander, W.J. [1984] Plane wave reflection coefficients for gas sands at non-normal angles of incidence. *Geophysics* **49**, 1637–1648.
Pemex Exploracion and Produccion [2000] *Las Reservas de Hidrocarburas de Mexico*. Pemex publication.
Pica, A., Diet, J., and Tarantola, A. [1990] Nonlinear inversion of seismic reflection data in a laterally invariant medium. *Geophysics* **55**, 284–292.
Rauch, M. and Craig, A. [1998] AVO behaviour at the top of a Class-4 sand – a case study of the Maitland-1 well. *60th EAGE Conference, Leipzig, Germany,* Extended Abstracts, paper 2-10.
Rauch-Davies, M. and Portniaguine, O. [2004] Elastic attribute generation from 3 points elastic inversion. *Offshore Technology Conference, Houston,* Paper 16731.
Rivenaes, J.C., Otterlei, C., Zachariassen, E., Dart, C., and Sjoholm, J. [2005] A 3D stochastic model integrating depth, fault, and property uncertainty for planning robust wells, Njord Field, offshore Norway. *Petroleum Geoscience* **11**, 57–65.
Robinson, N., Ford, A., Howie, J., Manley, D., Riviere, M., Stewart, S., and Thomas, R. [2005] 4D time-lapse monitoring of Chirag field. *The Leading Edge* **24**, 928–932.
Roden, R., Forrest, M., and Holeywell, R. [2005] The impact of seismic attributes on prospect risk analysis. *The Leading Edge* **24**, 706–711.
Ross, C.P. [2000] Effective AVO crossplot modelling: A tutorial. *Geophysics* **60**, 1398–1408.
Russell, B.H., Hedlin, K., Hilterman, F.J. and Lines, L.R. [2003] Fluid property discrimination with AVO: A Biot-Gassmann perspective. *Geophysics* **68**, 29–39.
Rutherford, S.R. and Williams, R.H. [1987] Amplitude-versus-offset variations in gas sands. *Geophysics* **54**, 680–688.
Sheriff, R.E. [2002] *Encyclopedic Dictionary of Exploration Geophysics*, 4th edn. SEG, Tulsa.
Shuey, R.T. [1985] A simplification of the Zoeppritz equations. *Geophysics* **50**, 609–614.
Skelt, C. [2004] Fluid substitution in laminated sands. *The Leading Edge* **23**, 485–488.
Smith, J.C. and Gidlow, P.M. [1987] Weighted stacking for rock property estimation and detection of gas. *Geophysical Prospecting* **35**, 993–1014.
Smith, J.C. and Sutherland, R.A. [1996] The fluid factor as an AVO indicator. *Geophysics* **61**, 1425–1428.
Tarantola, A. [1984] Inversion of seismic reflection data in the acoustic approximation. *Geophysics* **49**, 1259–1266.
Tarantola, A. [1986] A strategy for non-linear elastic inversion of seismic reflections data. *Geophysics* **51**, 1893–1903.
Tatham, R.H. [1982] Vp / Vs and lithology. *Geophysics* **47**, 336–344.
Todorovic-Marinic, D., Larson, G., Gray, D., Cheadle, S., Souleand, G., and Zheng, Y. [2004] Identifying vertical productive fractures in the Narraway gas field using the envelope of the anisotropic gradient. *First Break* **22**, 10, 45 – 50.
Tsuneyama, F., Takahashi, I., Nishida, A. and Okamura, H. [2003] Vp/Vs ratio as a rock frame indicator for a carbonate reservoir. *First Break* **21**, 7, 53-58.
Veeken, P.C.H [2006] *Seismic Stratigraphy, Basin Analysis and Reservoir Characterisation*. Handbook of Geophysical Exploration Series (eds K. Helbig and S. Treitel). Elsevier Scientific Publications (in press).
Veeken, P.C.H. and Da Silva, M. [2004] Seismic inversion and some of their constraints. *First Break* **22**, 6, 47–70.
Veeken, P.C.H., Rauch, M., Gallardo, R., Guzman E., and Vila Villasenor R. [2002] Seismic inversion of the Fortuna National 3D survey, Tabasco, Mexico. *First Break* **20**, 287–294.
Verm, R. and Hilterman, F. [1995] Lithology colour coded seismic sections, the calibration of AVO crossplotting to rock properties. *The Leading Edge* **14**, 847–853.
Whitcombe, D., Connolly, P., Reagan, R., and Redshaw, T. [2000] Extended elastic impedance for fluid and lithology prediction. *70th SEG Meeting, Calgary, Canada,* Expanded Abstracts, 138–141.
Wigger S., Bailey, J., Larsen, M. and Wallace, M. [1997] Ha'py Field: A Pliocene bright spot example from the Nile Delta, Egypt. *The Leading Edge* **16**, 1827–1829.
Williams, M. and Jenner, E. [2002] Interpreting seismic data in the presence of azimuthal anisotropy; or azimuthal anisotropy in the presence of the seismic interpretation. *The Leading Edge* **21**, 771–774.
Yilmaz, O. [2001] *Seismic data analysis*. SEG Publications, Tulsa.
Zoeppritz, K. [1919] On the reflection and propagation of seismic waves. Erdbebenwellen VIIB, Gottinger Nachrichten I, pp. 66–84.

KMS Technologies – KJT Enterprises Inc.
6420 Richmond Ave., Suite 610
Houston, Texas, 77057, USA
Tel: 713.532.8144

info@kmstechnologies.com

Please visit us
http://www.kmstechnologies.com//